Structural Characteristics of the Plasmid-Encoded Toxin from Enteroaggregative *Escherichia coli*[†]

Patricia Scaglione,[‡] Kathleen N. Nemec,[‡] Kaitlin E. Burlingame,[‡,§] Agnieszka Grabon,[‡] Jazmin Huerta,[||] Fernando Navarro-Garcia,[||] Suren A. Tatulian,[⊥] and Ken Teter*[,‡]

Department of Molecular Biology and Microbiology, Burnett School of Biomedical Science, College of Medicine, University of Central Florida, 12722 Research Parkway, Orlando, Florida 32826, Department of Cell Biology, Cinvestav-Zacatenco, Ap. Postal 14-740, 07000 México, DF, Mexico, and Department of Physics, University of Central Florida, 4000 Central Florida Boulevard, Orlando, Florida 32816

Received May 12, 2008; Revised Manuscript Received July 16, 2008

ABSTRACT: Intoxication by the plasmid-encoded toxin (Pet) of enteroaggregative *Escherichia coli* requires toxin translocation from the endoplasmic reticulum (ER) to the cytosol. This event involves the quality control system of ER-associated degradation (ERAD), but the molecular details of the process are poorly characterized. For many structurally distinct AB-type toxins, ERAD-mediated translocation is triggered by the spontaneous unfolding of a thermally unstable A chain. Here we show that Pet, a non-AB toxin, engages ERAD by a different mechanism that does not involve thermal unfolding. Circular dichroism and fluorescence spectroscopy measurements demonstrated that Pet maintains most of its secondary and tertiary structural features at 37 °C, with significant thermal unfolding only occurring at temperatures ≥50 °C. Fluorescence quenching experiments detected the partial solvent exposure of Pet aromatic amino acid residues at 37 °C, and a cell-based assay suggested that these changes could activate an ERAD-related event known as the unfolded protein response. We also found that HEp-2 cells were resistant to Pet intoxication when incubated with glycerol, a protein stabilizer. Altogether, our data are consistent with a model in which ERAD activity is triggered by a subtle structural destabilization of Pet and the exposure of Pet hydrophobic residues at physiological temperature. This was further supported by computer modeling analysis, which identified a surface-exposed hydrophobic loop among other accessible nonpolar residues in Pet. From our data it appears that Pet can promote its ERAD-mediated translocation into the cytosol by a distinct mechanism involving partial exposure of hydrophobic residues rather than the substantial unfolding observed for certain AB toxins.

The plasmid-encoded toxin (Pet[1]) of enteroaggregative *Escherichia coli* is a serine protease autotransporter of the *Enterobacteriaceae* (SPATE). Its eukaryotic target is the actin-binding protein α-fodrin (*1*). When Pet cleaves α-fodrin in the target cell cytosol, the organization of the actin cytoskeleton is disrupted. The loss of actin filament structure then results in cell rounding and detachment from the substratum. In the intestinal epithelium of an intoxicated mammal, these effects compromise the integrity of the epithelial monolayer and produce a potentially life-threatening case of diarrhea (*2, 3*).

Members of the SPATE family exhibit diverse functions, but all SPATEs contain the three characteristic domains of an autotransporter: the amino-terminal signal peptide, the mature protein, and the carboxy-terminal β-barrel structure (*4*). The signal peptide targets the nascent protein for delivery to the periplasmic space and is proteolytically removed from the toxin at this site. The mature protein (also called the passenger domain) contains a catalytic N-terminal domain that includes the canonical GDSGSPL serine protease motif of the SPATEs, followed by an extensive β-helix structural motif. The movement of the passenger domain through the bacterial outer membrane is mediated by the pore-forming β-barrel structure of the SPATE. Membrane-anchored passenger domains remain covalently linked to β-barrel structure, whereas secreted passenger domains are proteolytically nicked and separated from the extracellular face of the β-barrel. Few studies have considered how the structure of the secreted passenger domain affects host−toxin interactions. In this work we examined how the structure of the Pet passenger domain could influence its entry into the host cell cytosol.

The 104 kDa passenger domain of Pet (hereafter simply referred to as Pet) is secreted into the extracellular milieu and enters the target eukaryotic cell by receptor-mediated,

[†] This work was supported by NIH Grant R01 AI073783 to K.T. and by grants from Consejo Nacional de Ciencia y Tecnologı´a de México (CONACYT Grants 60714 and C02-44660) to F.N.-G.

* To whom correspondence should be addressed. Tel: (407) 882-2247. Fax: (407) 384-2062. E-mail: kteter@mail.ucf.edu.

[‡] College of Medicine, University of Central Florida.

[§] A student at Lake Brantley High School, Altamonte Springs, FL.

[||] Cinvestav-Zacatenco.

[⊥] Department of Physics, University of Central Florida.

[1] Abbreviations: CD, circular dichroism; CT, cholera toxin; ER, endoplasmic reticulum; ERAD, ER-associated degradation; FTIR, Fourier transform infrared; K_{SV}, Stern−Volmer constant; NaPi, sodium phosphate; Pet, plasmid-encoded toxin; PT, pertussis toxin; SPATE, serine protease autotransporter of the *Enterobacteriaceae*; T_m, transition midpoint; UPR, unfolded protein response; λ_{max}, maximum emission wavelength.

10.1021/bi8008714 CCC: $40.75
Published on Web 08/15/2008

clathrin-dependent endocytosis (*5*). Internalized Pet then moves from the endosomes to the Golgi and from the Golgi to the endoplasmic reticulum (ER) by vesicle traffic (*6, 7*). Before entering the cytosol, ER-localized Pet associates with the Sec61 translocon pore (*6*). Sec61 is active in ER-associated degradation (ERAD), a quality control system that recognizes misfolded or misassembled proteins in the ER and exports them to the cytosol for disposal (*8*). ERAD also facilitates the ER-to-cytosol export of Pet, as mutant cell lines with aberrant ERAD activity display increased resistance to Pet intoxication (*6*). The structural feature(s) of Pet which engage the ERAD system are unknown.

Like Pet, many AB toxins move from the cell surface to the ER and from the ER to the cytosol (*9*). These AB toxins, which include cholera toxin (CT), pertussis toxin (PT), and ricin, share a common structural organization that consists of an enzymatic A subunit and a cell-binding B subunit. Holotoxin disassembly occurs in the ER, and only the catalytic A subunit enters the cytosol. Thermal instability in the dissociated A chain generates an unfolded toxin conformation that most likely triggers its ERAD-mediated translocation to the cytosol (*10*−*12*). An absence or paucity of lysine residues in the toxin A chain protects it from the ubiquitin-dependent proteasomal degradation that usually accompanies ERAD-mediated export to the cytosol (*13*−*15*).

Pet does not have an AB structural organization, and it enters the cytosol as an intact 104 kDa protein (*6*). The large size of Pet also distinguishes it from the 20−30 kDa toxin A chains, as do the numerous lysine residues in Pet. Because Pet is structurally distinct from the A chains of other ER-translocating toxins, we predicted that it activates ERAD by a process distinct from the AB toxin mechanism. Our data support this hypothesis and indicate that Pet can promote its ERAD-mediated translocation into the cytosol without the substantial loss of structure observed for some AB-type, ER-translocating toxins.

EXPERIMENTAL PROCEDURES

Pet Purification. Pet was purified as previously described (*6*). Lyophilized Pet was dissolved in double distilled H_2O and sterilized with a 2 μm syringe filter before loading onto a hi-load 16/60 75 Superdex size-exclusion column (GE Healthcare, Piscataway, NJ). An ÄKTA purifier (GE Healthcare) was used to fractionate samples in elution buffer (20 mM Tris pH 7.4 + 25 mM KCl) at a rate of 0.5 mL/min. Peak fractions were collected and concentrated using YM30 concentrators (Millipore, Bedford, MA). Toxin activity in the peak fractions was confirmed by the morphological effect (i.e., cell rounding and substratum detachment) observed in CHO cells exposed to 40 μg/mL of the fractionated material for 16−24 h.

Circular Dichroism (CD). Purified Pet was placed in 20 mM sodium phosphate (NaPi) buffer (pH 7.0) at a final protein concentration of 0.31 mg/mL. Measurements were performed with a 0.4 cm path length rectangular quartz cuvette and a J-810 spectrofluoropolarimeter (Jasco Corp., Tokyo, Japan). Thermal unfolding was carried out in the temperature range of 18 to 60 °C, and samples were allowed to equilibrate for 4 min at each temperature before measurement. CD spectra were recorded either from 200 to 250 nm (far-UV CD) or from 245 to 300 nm (near-UV CD) and averaged from 5 scans. The observed ellipticity was converted to mean residue molar ellipticity, $[\theta]$, in units of degrees × cm^2 × dmol^{-1} using $[\theta] = \theta_{obs}/cn_{res}l$, where θ_{obs} is the measured ellipticity in millidegrees, c is the molar concentration of the protein, n_{res} is the number of amino acid residues in the protein, and l is the optical path length in millimeters.

Fluorescence Spectroscopy. Pet tryptophan residues were excited at 280 nm, and the fluorescence emission was measured between 300 and 400 nm. Fluorescence intensity in the 325−345 nm region is dominated by emission from tryptophan with a minor contribution from tyrosine because the quantum yield of tyrosine is much lower and tyrosine emission occurs in the 300−310 nm region (*16*). Protein concentration for the purified toxin was 0.45 mg/mL in 20 mM NaPi buffer (pH 7.0). The excitation and emission slits were set to 1 and 10 nm, respectively, and the spectral resolution was 1 nm. Measurements were taken in a 0.4 cm path length cuvette with a J-810 spectrofluoropolarimeter during a stepwise increase in temperature from 18 to 60 °C. To calculate transition midpoints (T_m) for loss of fluorescence intensity and for a red shift in the maximum emission wavelength (λ_{max}), the temperature-dependent protein unfolding data were analyzed as previously described (*11, 12*).

For experiments involving the quenching of fluorescence intensity, Pet tryptophan residues were excited at 290 nm and the fluorescence emission was measured between 300 and 400 nm. Other experimental parameters were identical to the conditions described in the preceding paragraph. After sample measurement at the indicated temperature, 1 μL of a 1 M acrylamide solution was added to the 200 μL toxin sample. Another measurement was then taken after 2 min of sample equilibration. This procedure of acrylamide addition was repeated 12 times. In parallel control experiments the same protocol was followed except 1 μL additions of 20 mM NaPi (pH 7.0) were added in the place of acrylamide. Independent experiments were performed with toxin samples incubated at 4 °C, 33 °C, 37 °C, 41 °C, 55 °C, and 60 °C.

Other Assays. Analysis of Pet toxicity by confocal microscopy was performed as described in ref *1*. The cell rounding Pet toxicity assay was performed as described in ref *6*; the unfolded protein response (UPR) assay was performed as described in ref *17*; and the protease sensitivity assay was performed as described in ref *12*. For the protease sensitivity assay, glycerol was removed from the stock sample of α-fodrin (Sigma-Aldrich, St. Louis, MO) by dialysis before use in the assay.

Computer Modeling. Hemoglobin protease, a SPATE with a solved crystal structure (PDB 1WXR) (*18*), was used as a template to model the structure of Pet with the ESyPred3D online structure prediction server (*19*) found at the ExPASy Web site (http://www.fundp.ac.be/sciences/biologie/urbm/bioinfo/espred/). The passenger domains of Pet and hemoglobin protease share 26% sequence identity and 43% sequence similarity. Space-filling and ribbon structures were generated using WebLab Viewer Lite.

RESULTS

Conformational Stability of Pet. It has been reported that Pet is inactivated by a 15 min incubation at 75 °C (*3*). We

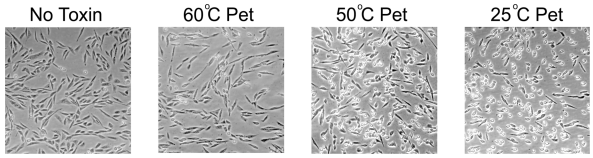

FIGURE 1: Heat inactivation of Pet. Pet was heated for 10 min at 60 °C, 50 °C, or 25 °C. Either toxin-free media or Pet-containing media (40 μg/mL) were then added to CHO cells for 10 h at 37 °C.

Table 1: Computational Predictions of Toxin Stability[a]

toxin	instability index	classification
Pet	18.5	stable
ricin A	38.8	stable
CTA1	41.6	unstable
PTS1	45.2	unstable

[a] Protein instability data for Pet and for the A chains of ricin, cholera toxin (CTA1), and pertussis toxin (PTS1) were obtained from the ProtParam function of ExPASy-SWISS-PROT. An instability index value greater than 40 is indicative of protein instability. The predicted A chain stabilities were consistent with experimental data from three studies which collectively indicated a relative stability order of ricin A > CTA1 > PTS1 (*10*−*12*). It should be noted that an interaction with negatively charged phospholipids is thought to further destabilize ricin A chain before its export from the ER to the cytosol (*34*).

further noted that Pet is inactivated by a 10 min incubation at 60 °C but retains substantial activity after a 10 min incubation at 50 °C and is active at lower temperatures (Figure 1). These data indicate that Pet is much more stable than the A chains of AB-type, ER-translocating toxins, which was consistent with protein instability estimates obtained from ExPASy-SWISS-PROT (Table 1). To directly confirm the thermal stability of Pet, the toxin was purified for structural studies involving far-UV CD. A Coomassie-stained gel of the purified toxin detected a single 104 kDa protein which corresponded to the molecular mass of Pet (data not shown). The purified toxin was placed in 20 mM NaPi buffer, and far-UV CD measurements of Pet secondary structure were then taken during a stepwise increase in temperature from 18 to 60 °C (Figure 2). At low temperatures, the CD spectra exhibited a single minimum around 217 nm which corresponded to the extensive β-sheet content of Pet (Figure 2A). A gradual loss of CD signal related to the β-sheet structure occurred as the temperature increased from 18 to 52 °C, and a dramatic loss of signal occurred at temperatures above 52 °C (Figure 2B). Using a chemical denaturant, Renn and Clark (*20*) likewise documented a two-step transition to the final unfolded state of Pet. The thermal denaturation of Pet secondary structure was irreversible as demonstrated by measurements taken during stepwise sample cooling from 60 to 18 °C (Figure 2B). Pet only lost 23% of its initial secondary structure at 37 °C, which was substantially different from the thermal stabilities of other structurally distinct ER-translocating toxins: 88% of the secondary structure for the catalytic S1 subunit of PT and 44% of the secondary structure for the catalytic A1 subunit of CT are lost at 37 °C (*11, 12*). The secondary structure of Pet was thus relatively stable at physiological temperature, with major thermal unfolding only occurring at temperatures above 50 °C.

Fluorescence spectroscopy and near-UV CD were used to monitor the thermal stability of Pet tertiary structure (Figure 3). Purified Pet was placed in NaPi buffer, and measurements of tryptophan fluorescence were taken during a stepwise increase in temperature from 18 to 60 °C. Pet contains seven tryptophan residues that dominate its fluorescence spectra (Figure 3A). The fluorescence intensity gradually decreased with increasing temperature from 18 to 37 °C, and then a steeper and sigmoidal decrease in fluorescence intensity occurred at higher temperatures (Figure 3A, inset). This suggested the involvement of at least two distinct thermal effects. The initial gradual decrease in fluorescence intensity most likely resulted from nonradiative deexcitation of the fluorophores because of internal conversion and, with increasing temperature, an increased rate of collisions with the solvent molecules. These effects are independent of conformational changes in the protein (*21, 22*). A combination of this "trivial" thermal deexcitation and an actual destabilization of protein tertiary structure provides the most reasonable interpretation of the steeper and sigmoidal quenching of Pet fluorescence that occurred at temperatures above 37 °C. By fitting the higher-temperature wing of the thermal profile of Pet fluorescence intensity with a simulated curve, changes in the tertiary structure could be described as a thermal transition with a T_m of 46 °C.

A red shift in the λ_{max} is indicative of a change in protein compaction and the exposure of tryptophans to water, followed by partial loss of the excited-state energy due to solvent relaxation (*22*). For Pet, the red shift occurred above 40 °C and exhibited a sigmoidal transition with a T_m of 50 °C (Figure 3B). Different molecular mechanisms for changes in fluorescence intensity and λ_{max} (e.g., quenching via internal conversion and Stokes shift, respectively) can explain the slightly different T_m values and transition curves for these two parameters (*21, 22*). However, both parameters suggested that physiological temperatures do not induce changes in the tertiary structure of Pet which would generate significant solvent access to tryptophan residues.

Near-UV CD spectroscopy was used as a complementary method to probe the temperature dependence of Pet tertiary structure (Figures 3C,D). This method is very sensitive to changes in protein tertiary structure and associated changes in the conformation and microenvironment of aromatic amino acid side chains (*23*−*25*). The near-UV CD spectra of Pet showed two major components around 270 nm and 280−288 nm (Figure 3C). A weaker component was also present at 250−260 nm. Near-UV CD bands around 250 nm are generated by $\pi-\pi^*$ transitions of tyrosine side chains and by the $n-\sigma^*$ transition of disulfides, while both tyrosine and tryptophan can contribute to the signal around 280 nm (*24, 25*). Phenylalanine generates weaker signals at shorter wavelengths (*24, 25*). Pet has two cysteine residues that are unlikely to form a disulfide bond, so its near-UV CD spectra mainly results from the contributions of twenty-nine tyrosine and seven tryptophan residues. The three near-UV CD components at 250, 270, and 280 nm all exhibited a biphasic dependence on temperature: the band intensities gradually changed from negative values to nearly zero or positive values as the temperature increased from 18 °C to 40−45 °C, and then changed to the opposite direction at higher temperatures (Figure 3D). The change in CD signals from 18 °C to 40−45 °C can be interpreted as a gradual destabilization, or opening, of Pet tertiary structure, accompanied with increased flexibility of tyrosine and tryptophan side chains. Partial restoration of the signal at temperatures >45 °C might result from

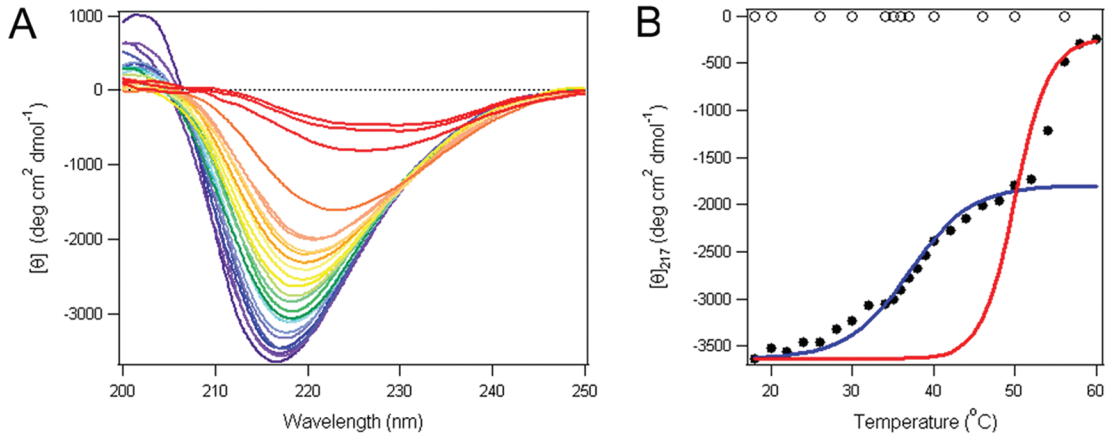

FIGURE 2: Thermal stability of Pet secondary structure. (A) Far-UV CD spectra of Pet were measured during a stepwise increase in temperature. The change in color from blue to red corresponds to a change in temperature from 18 to 60 °C. (B) Alterations to the secondary structure of Pet ($[\theta]_{217}$) were plotted as a function of temperature (filled circles). Also shown are the $[\theta]_{217}$ signals for a Pet sample that was cooled to 18 °C after heating to 60 °C (open circles). The overall temperature dependence of $[\theta]_{217}$ is fitted with two simulated curves using transition midpoint values of $T_m = 37$ °C (blue curve) and $T_m = 55$ °C (red curve).

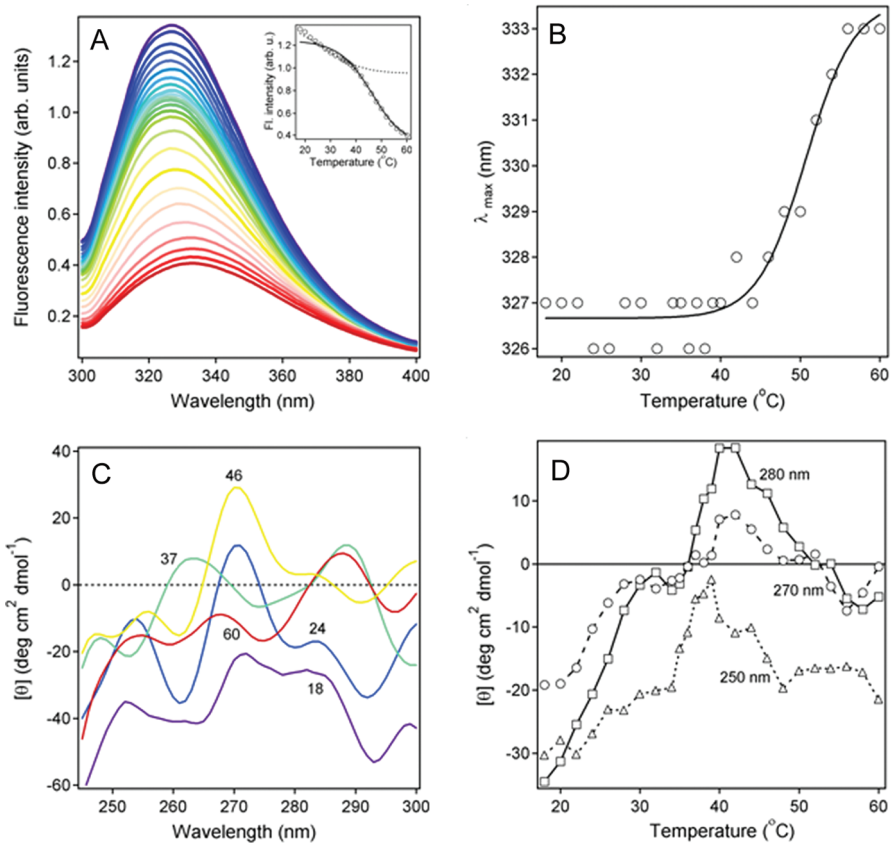

FIGURE 3: Thermal stability of Pet tertiary structure. (A) The fluorescence spectra of Pet were measured during a stepwise increase in temperature. The change in color from blue to red corresponds to a change in temperature from 18 to 60 °C. Temperature-dependent alterations to the fluorescence intensity are shown in the inset. The initial gradual decrease in fluorescence intensity is plotted as a dashed line, and the temperature-induced sigmoidal change in the protein tertiary structure is plotted as a solid line using $T_m = 46$ °C. (B) Alterations to the λ_{max} of Pet tryptophan fluorescence were plotted as a function of temperature. The circles are the data points, and the solid line was simulated using $T_m = 50$ °C. (C) Near-UV CD spectra of Pet were measured during a stepwise increase in temperature from 18 to 60 °C. Select spectra (18 °C, 24 °C, 37 °C, 46 °C, and 60 °C) are shown for clarity; the colors correspond to the temperature coloring scheme used for presentation of other CD and fluorescence data. (D) Alterations to the near-UV CD bands at 250, 270, and 280 nm are plotted as functions of temperature.

protein−protein hydrophobic interactions, probably because of exposed nonpolar residues. The appearance of chiral C_α atoms from surrounding molecules near surface-exposed tyrosine and tryptophan residues would mimic the formation of a more compact tertiary structure, as at the lower temperatures, and would result in a biphasic temperature dependence of the CD signal.

Comparison of the near- and far-UV CD data shows that the Pet tertiary structure undergoes a steeper thermal destabilization than the secondary structure when the protein is heated from 18 °C to 40−45 °C. However, our fluorescence spectroscopy data demonstrated that this destabilization does not produce a toxin conformation with solvent-exposed tryptophan residues until the temperature is raised above 40

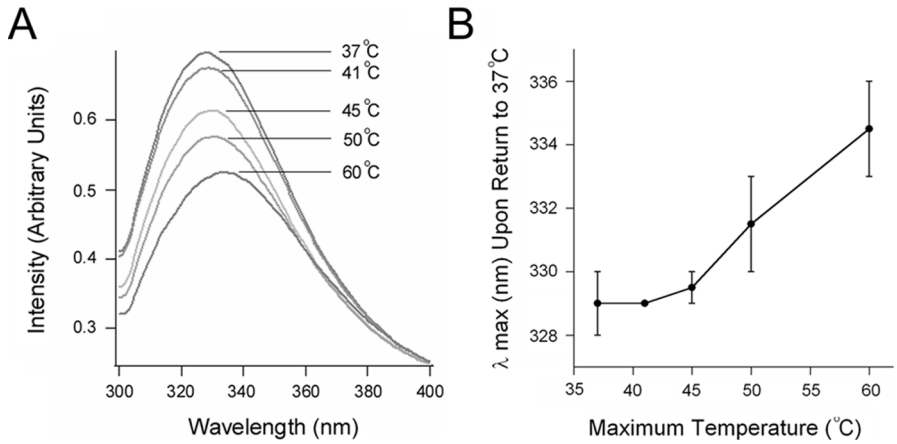

FIGURE 4: Irreversible disordering of Pet tertiary structure. The fluorescence spectra of Pet were measured at 37 °C after cooling from the indicated temperatures. One of two experiments is shown in (A); the average ± range of both experiments is shown in (B).

°C (Figure 3B). The red shift for λ_{max} of tryptophan fluorescence also indicated that a substantial loss of protein compaction only occurs at temperatures above 50 °C and is concurrent with the major thermal destabilization of Pet secondary structure. Pet therefore appears to undergo some temperature-dependent alterations to its secondary and tertiary structures at physiological temperature, but dramatic thermal unfolding of the toxin only occurs at higher temperatures. In contrast, the catalytic subunits of PT and CT are in unfolded conformations at 37 °C (*11, 12*).

Refolding of Pet Tertiary Structure. Ricin A chain may trigger the ERAD system by a thermal ratchet mechanism in which minor irreversible changes to the toxin structure accumulate due to thermal fluctuations (*10*). These changes eventually produce an unfolded protein at temperatures that normally support the folded toxin conformation. To determine if Pet could activate the ERAD system by a similar mechanism, we examined the refolding of Pet tertiary structure by fluorescence spectroscopy (Figure 4). Purified toxin was heated with a stepwise increase in temperature to 41 °C. The sample was then cooled back to 37 °C, and the fluorescence emission spectrum was recorded at 37 °C. This process was repeated for separate toxin samples that had been heated to maximum temperatures of 45 °C, 50 °C, or 60 °C. For reference, the fluorescence emission spectrum of a toxin sample that was only heated to 37 °C was recorded as well. A transient rise in temperature up to 45 °C did not affect the fluorescence emission spectrum of Pet upon sample cooling to the 37 °C. In contrast, heating Pet to 50 or 60 °C resulted in a substantial red shift which was not reversed upon sample cooling and measurement at 37 °C. The loss of Pet tertiary structure at these temperatures was therefore irreversible. As relatively high temperatures were required for the irreversible unfolding of Pet tertiary structure, a thermal ratchet mechanism in the physiological temperature range is unlikely to account for Pet activation of the ERAD system.

Effect of Glycerol, a Chemical Chaperone, on In Vivo Pet Activity. Our biophysical data demonstrated that Pet is in a folded conformation at 37 °C. However, most proteins require at least partial unfolding in order to move from the ER to the cytosol through the pore of the Sec61 translocon. Unfolding is facilitated by ER-localized chaperones which comprise part of the ERAD system. To determine if protein unfolding is required for Pet to access the cytosol, we performed a Pet toxicity assay with glycerol-treated HEp-2 cells (Figure 5). Glycerol is a chemical chaperone that stabilizes protein structures and prevents intoxication with ricin (*26, 27*). An inhibition of Pet toxicity in glycerol-treated cells would therefore suggest that an unfolding step may be necessary for Pet to reach its cytosolic target.

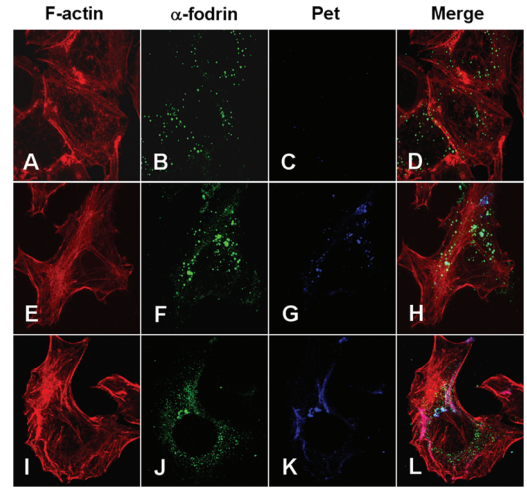

FIGURE 5: Effect of glycerol on Pet toxicity. After a 2 h exposure to 7% glycerol and/or 37 μg of Pet/mL, HEp-2 cells were fixed and exposed to rhodamine-phalloidin, anti-α-fodrin antibodies, and anti-Pet antibodies. Fluorescein-labeled secondary antibodies were used to visualize α-fodrin, while CY5-labeled secondary antibodies were used to visualize Pet. (A−D) Cells were incubated with glycerol in the absence of Pet. (E−H) Cells were incubated with Pet in the absence of glycerol. (I−L) Cells were incubated with both glycerol and Pet. Colocalization of α-fodrin and Pet is indicated by the aquamarine color in the merged images.

Prolonged exposure to glycerol results in cell rounding, so we could not use this phenotype to track Pet toxicity in glycerol-treated cells. Instead, we monitored the intracellular redistribution of α-fodrin that occurs after it is cleaved by cytosolic Pet. Unintoxicated cells incubated with 7% glycerol for 2 h displayed an intact actin cytoskeleton and the typical punctate distribution of α-fodrin that has been previously reported (Figures 5A−D) (*1*). Untreated cells exposed to 37 μg of Pet/mL for 2 h also displayed an intact cytoskeleton, but α-fodrin was clearly redistributed into intracellular aggregates that colocalized with Pet (Figures 5E−H). Previous work has shown that Pet can be detected in the cytosol after 2 h of intoxication, but it does not affect the actin cytoskeleton in this time frame (*1, 6*). Aggregation of

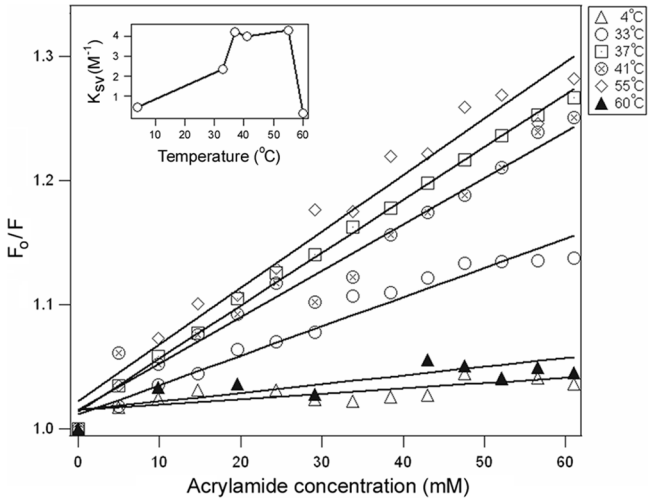

FIGURE 6: Quenching of Pet tryptophan fluorescence. Fluorescence spectra were measured at each indicated temperature with two parallel samples of Pet: one in which an increasing volume of acrylamide was added to the sample (F), and another in which an increasing volume of buffer was added to the sample (F_o). The ratio of the maximum emission wavelength for each matched set of samples (F_o/F) is plotted as function of acyrlamide concentration. For the inset, K_{SV} values are plotted as functions of temperature.

α-fodrin was nearly absent in glycerol-treated cells exposed to Pet (Figures 5I−L). Very little colocalization between α-fodrin and Pet was detected in the glycerol-treated cells; Pet instead accumulated in tubularized structures that tracked along the actin microfilaments. As the ER can be closely associated with the actin cytoskeleton (*28*), the tubularized Pet-containing structures most likely represent regions of the ER. Our findings indicate that glycerol treatment prevents Pet intoxication, most likely by blocking Pet exit from the endomembrane system. Thus, although Pet does not undergo spontaneous unfolding at physiological temperature, at least partial unfolding in the ER is likely required for Pet to move into the cytosol and reach its cytosolic target.

The Hydrophobic Properties of Pet. Temperature-induced changes to the tertiary structure of Pet were monitored in Figure 3, but these experiments did not determine the surface hydrophobicity of native Pet. Fluorescence quenching experiments were accordingly used to examine the hydrophobic characteristics of Pet (*21*). Pet could activate the ERAD system without the need for a substantial structural change if its native conformation contained surface-exposed hydrophobic residues.

In order to test this hypothesis, flourescence quenching experiments were performed with Pet samples incubated at 4 °C, 33 °C, 37 °C, 41 °C, 55 °C, or 60 °C (Figure 6). Addition of up to 60 mM acrylamide, a water-soluble fluorescence quencher, had negligible effect on Pet fluorescence intensity when the toxin was incubated at 4 °C. This indicated that tryptophans and other aromatic amino acid residues were effectively shielded from the solvent at low temperatures. However, some quenching was detected when Pet was incubated at 33 °C, and a greater level of quenching was observed when Pet was incubated at 37 °C. No further quenching was detected for the 41 and 55 °C toxin samples. Acrylamide quenching of Pet fluorescence decreased to a negligible level at 60 °C, similar to that observed at 4 °C. The inset to Figure 6 shows the Stern−Volmer constants (K_{SV}; the quenching efficiency of acrylamide) as a function

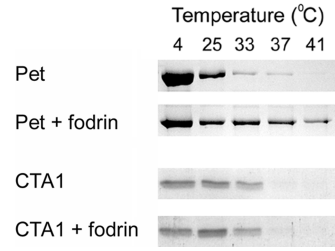

FIGURE 7: Pet protease sensitivity. Pet or the reduced CTA1/CTA2 heterodimer was incubated for 1 h at the indicated temperatures in the absence or presence of α-fodrin. Toxin samples were then shifted to 4 °C and exposed to thermolysin for 1 h before resolution by SDS−PAGE with Coomassie staining.

of temperature, which describes the temperature-dependence of acrylamide quenching in a quantitative manner.

Acrylamide quenching experiments detected an 8-fold increase in quenching efficiency as the temperature increased from 4 to 37 °C. This was consistent with the gradual thermal destabilization of Pet tertiary structure as detected by changes to the near-UV CD signals (Figures 3C,D). However, as judged from the temperature dependence of λ_{max} of tryptophan fluorescence, the loss of protein compaction and solvent exposure of tryptophans did not occur until Pet was heated above 40 °C (Figures 3A,B). These collective results suggest that physiological temperatures induce a subtle destabilization of Pet tertiary structure which allows stronger quenching by a water-soluble quencher without extensive exposure of tryptophans to the solvent. The nearly identical K_{SV} values obtained at 37 °C, 41 °C, and 55 °C further indicated that the maximal access of acrylamide to tryptophan residues occurred at or around the physiological temperature of 37 °C. The sharp decline in acrylamide quenching at 60 °C most likely resulted from protein denaturation and aggregation. This event, which was consistent with (i) the irreversible disordering of Pet secondary and tertiary structures at 60 °C (Figures 2B and 4) and (ii) the biphasic temperature dependence of the near-UV CD signals (Figure 3D), would block acrylamide access to the fluorescent amino acid residues of Pet and would thereby prevent fluorescence quenching. Temperature-induced aggregation of Pet at high temperatures has been supported by experiments using Fourier transform infrared (FTIR) spectroscopy, which suggested formation of intermolecular β-sheet structures and concomitant loss of intramolecular β-sheet structures at temperatures above 55 °C (Supporting Information Figures S1−S3).

As an alternative method to demonstrate the hydrophobic properties of Pet, we employed a thermolysin protease sensitivity assay (Figure 7). Thermolysin cleaves peptide bonds to the amino-terminal side of the hydrophobic amino acids valine, alanine, isoleucine, leucine, phenylalanine, and methionine. Sensitivity to thermolysin digestion would therefore indicate that Pet contains accessible, surface-exposed hydrophobic residues other than the tryptophans detected by our fluorescence quenching experiment.

Samples of Pet were preincubated for 1 hour at 4 °C, 25 °C, 33 °C, 37 °C, or 41 °C. The toxin samples were then placed on ice and exposed to thermolysin for another 1 hour. Since all digestions were performed at 4 °C, any differences in protease sensitivity must have resulted from temperature-induced conformational changes that occurred during the

preincubation stage. Pet samples preincubated at temperatures ≥33 °C were highly susceptible to proteolysis with thermolysin: the toxin sample preincubated at 41 °C was completely digested by thermolysin, and only minor amounts of toxin remained from the 33 and 37 °C samples. Some proteolysis of the 25 °C toxin sample also occurred. These results were consistent with our CD and fluorescence data which demonstrated a mildly disturbed secondary structure (Figure 2B), gradual destabilization of tertiary structure (Figures 3C,D), and a partial opening of the tertiary fold of Pet (Figure 6) over a physiological temperature range. Interestingly, Pet was substantially protected from degradation when it was exposed to an equimolar concentration of α-fodrin. An interaction with its cellular target may thus induce a conformational change in Pet that alters the accessibility of its surface-exposed hydrophobic residues. Alternatively, α-fodrin may have acted as a competitive inhibitor to prevent an interaction between Pet and thermolysin. Future structure−function studies should distinguish between these possibilities.

For comparative purposes, the protease sensitivity assay was also performed with samples of a purified, reduced CTA1/CTA2 heterodimer. The catalytic CTA1 subunit dissociates from CTA2 in the presence of 10 mM β-mercaptoethanol, which mimics the normal holotoxin disassembly event that occurs in the ER (*12*). As previously reported, reduced CTA1 exhibited a temperature-dependent pattern of thermolysin sensitivity: it was in a protease-sensitive state when preincubated at temperatures ≥37 °C and in a protease-resistant state when preincubated at temperatures ≤33 °C (*12*). The presence of α-fodrin did not alter the pattern of protease sensitivity for reduced CTA1, thereby demonstrating the specificity of the inhibitory effect of α-fodrin on Pet proteolysis.

Pet Activation of the UPR. ERAD is a normal cellular process that continually clears the ER of misfolded or misassembled proteins. A secondary quality control system called the UPR is activated under conditions of cellular stress and/or when basal ERAD activity cannot effectively cope with the amount of misfolded proteins in the ER (*29*). Pet translocation involves ERAD, so the UPR might be triggered by Pet intoxication. To examine this possibility, we used a previously described reporter assay in which the expression of firefly luciferase is controlled by a UPR-inducible promoter (*17*). This assay could readily detect UPR activation after stress induction with thapsigargin, a Ca^{2+}-ATPase inhibitor that depletes the ER Ca^{2+} stores (Figure 8). A 10 h exposure to 60 μg of Pet/mL also led to activation of the UPR, although Pet concentrations of 40 or 20 μg/mL did not trigger the UPR (Figure 8). Productive intoxication occurs with 40 μg of Pet/mL (Figure 1), so the cytopathic activity of Pet did not appear to be responsible for UPR activation. Furthermore, a catalytically inactive S260I Pet mutant (*30*) was also able to trigger the UPR when applied to cells at a concentration of 60 μg/mL (Figure 8). UPR activation was thus linked to the Pet protein itself rather than to Pet activity. This was consistent with a translocation model in which Pet masquerades as a misfolded protein to trigger its ERAD-mediated export to the cytosol.

Computer Modeling of Pet Structure. As our fluorescence quenching and protease sensitivity data indicated solvent accessibility of Pet hydrophobic/aromatic amino acid residues

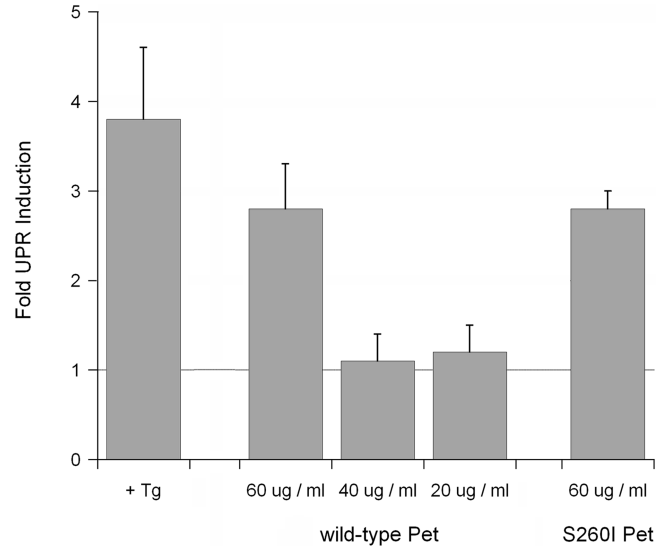

FIGURE 8: Pet induction of the UPR. A luciferase-based reporter assay was used to monitor UPR activation in CHO cells exposed to Pet for 10 h or to 200 nM thapsigargin (Tg) for 2 h. To calculate the extent of UPR induction, values from the experimental conditions were divided by the control value from untreated cells. The means ± standard errors of the means from 3−5 independent experiments per condition are shown.

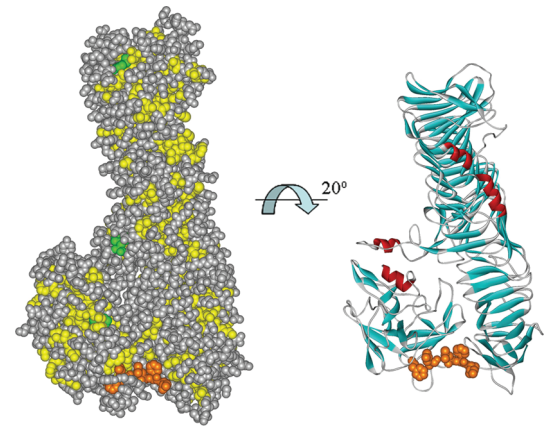

FIGURE 9: Surface-exposed hydrophobic residues of Pet. A space-filling diagram highlights the Pet tryptophan residues in green and the thermolysin-susceptible hydrophobic amino acid residues in yellow. The space-filling diagram was rotated on a 20° axis to distinguish the catalytic domain from the β-helix domain in the presented ribbon structure. For both space-filling and ribbon diagrams, orange space-filling molecules denote the hydrophobic amino acid residues (F_{297}, L_{305}, L_{308}, F_{309}, and I_{310}) located in the unstructured region of Pet linking the β-helix domain to the catalytic domain. In the ribbon diagram, β-sheets are highlighted in blue and α-helices are highlighted in red.

at 37 °C, we attempted to identify the location of these surface-exposed hydrophobic residues. A crystal structure of Pet is not available, but the structure of another SPATE (hemoglobin protease) has been determined (*18*). We therefore used the hemoglobin protease crystal structure as a template to model the structure of Pet with the ESyPred3D program from the ExPASy Proteomics tools Web site. Additional computer modeling was then used to identify potential surface-exposed hydrophobic residues in Pet that could trigger the ERAD mechanism (Figure 9). A space-filling diagram of Pet indicated that at least three tryptophan residues (Trp_{274}, Trp_{628}, and Trp_{985}; all numbering is from the first residue of the signal sequence) are partially acces-

sible to solvent. Trp_{403} and Trp_{860} are buried within the β-helix; Trp_{61} and Trp_{642} were not returned with the model coordinates. The three solvent-exposed tryptophan residues are unlikely to serve as the ERAD recognition motif because they are spatially segregated and only partially accessible to solvent. However, a different view was obtained when the space-filling model of Pet was used to map the hydrophobic residues susceptible to thermolysin cleavage. In this case, numerous clusters of solvent-exposed hydrophobic amino acid residues were identified. One such cluster of partially or fully exposed residues included F_{297}, L_{305}, L_{308}, F_{309}, and I_{310}. This particular hydrophobic region is of interest because it spans an exposed loop which connects the catalytic domain to the β-helix (Figure 9). This stretch of exposed hydrophobic residues lacks secondary structure and is a potential site for toxin−ERAD interactions.

DISCUSSION

The A subunits of at least three AB-type, ER-translocating toxins exhibit a common property of thermal instability that becomes apparent after holotoxin disassembly in the ER (*10*−*12*). Partial unfolding of the dissociated toxin A chain at physiological temperature could then identify it as a misfolded protein for ERAD-mediated export to the cytosol. Pet, in contrast, is a non-AB toxin that moves from the ER to the cytosol as an intact, 104 kDa protein (*6*). In this report our data demonstrates that Pet is a thermally stable protein within the physiological temperature range and must therefore trigger the ERAD export system by a means that is distinct from the AB toxin translocation mechanism.

Substantial disordering of Pet tertiary and secondary structure does not occur at 37 °C. However, the UPR is active in Pet-treated cells. This indicates that Pet can, without dramatic alterations to its native conformation, masquerade as a misfolded protein to trigger both ERAD and the UPR. CD, fluorescence quenching, and protease sensitivity assays indeed detected subtle temperature-dependent changes to the structure of Pet that were linked to the surface exposure of Pet hydrophobic amino acid residues. The homology-modeled structure of Pet identified numerous surface-exposed hydrophobic residues, and a potential candidate for the ERAD trigger was found in an exposed, unstructured hydrophobic region linking the β-helix domain to the catalytic domain. Future studies to define the Pet translocation domain will focus on this stretch of hydrophobic amino acids residues.

The temperature dependence of protein fluorescence involves various factors. Protein fluorescence intensity is determined by $\phi_F = k_F/\{k_F + k_{ic} + k_{is} + k_q[Q]\}$, where ϕ_F is the fraction of excited fluorophores that emit fluorescence with a rate constant k_F; k_{ic} is the rate constant of internal conversion; k_{is} is the rate constant of intersystem crossing; and k_q is the rate constant of direct quenching by a quencher at concentration [Q] (for more detail see ref *21*). An increase in k_{ic} with increasing temperature is believed to cause a decrease in protein fluorescence even in the absence of external quenchers (*21*). The temperature dependence of Pet fluorescence intensity shown in Figure 3A and Figure 4 thus involves at least two components: (i) the effect of k_{ic}, which may result from increased motional freedom of amino acid side chains without considerable changes in the protein backbone structure; and (ii) the effect of k_q that is likely related to changes in the protein tertiary structure. For the fluorescence quenching data of Figure 6, Pet samples were held at a single temperature as the concentration of acrylamide quencher increased. The changes to protein fluorescence intensity were therefore mainly due to the effect of k_q. The CD and fluorescence quenching data of Figures 2B and 6 identified changes in Pet ellipticity and fluorescence intensity at 33 and 37 °C, yet a red shift of λ_{max} did not occur until the temperature was above 40 °C. We conclude that Pet undergoes subtle structural changes at 33 and 37 °C but only becomes destabilized at temperatures above 40 °C when the λ_{max} undergoes a red shift. It is likely that these subtle structural changes help Pet masquerade as a misfolded protein for ERAD-mediated export to the cytosol. In contrast, the A chains of AB-type, ER-translocating toxins actually unfold before passage into the cytosol. Pet thus appears to activate the ERAD system by a process that is distinct from the AB toxin mechanism.

Our data consistently indicated that Pet tertiary structure becomes more open at 40 °C, but near-UV CD data implied the onset of intermolecular interactions at 40−45 °C while quenching data indicated protein aggregation above 55 °C. FTIR spectroscopy measurements also suggested the formation of intermolecular hydrogen bonds and protein aggregation at temperatures above 55 °C. Thus, the near-UV CD signal is apparently more sensitive to the microenvironment than either fluorescence quenching or FTIR spectroscopy. Conditions/temperatures which modulate the microenvironment of aromatic amino acid side chains and alter the CD signal upon the onset of protein aggregation do not necessarily prevent acrylamide from reaching the aromatic side chains and causing fluorescence quenching. Likewise, near-UV CD is sensitive to the microenvironment at intermolecular distances larger than those necessary for hydrogen bond formation and appearance of the respective low-frequency amide I component in the FTIR spectra. Although the onset of intermolecular interactions occurs at 40−45 °C (Figure 3D), Pet maintains some in vivo activity after heating to 50 °C (Figure 1) and does not undergo irreversible aggregation until the temperature is raised above 50 °C (Figures 2B, 4, 6, and S3). Altogether, these results indicate that Pet is in a relatively stable conformation at 37 °C and only undergoes dramatic structural alterations at significantly higher temperatures.

The N-terminal region of Pet that spans both the β-helix and the catalytic domain has a predicted width of 76 Å (Figure 9), but the Sec61 translocon pore has a maximum diameter of 60 Å (*31*). Thus, chaperone-assisted rearrangement of Pet structure is likely required for its passage from the ER to the cytosol. This possibility is supported by the inhibition of Pet intoxication in glycerol-treated cells. Unfolding of the Pet β-helix is unnecessary, as this structure is sufficiently narrow (50 Å predicted width) to pass through the translocon intact. Interestingly, the unstructured hydrophobic linker which may facilitate toxin−ERAD interactions is found within the 76 Å N-terminal region of Pet. Recruitment of ER chaperones to this putative ERAD interaction motif could consequently lead to localized unfolding of the one region in Pet that cannot pass through the Sec61 translocon in a folded state. Alternatively, ER chaperones could simply pivot the catalytic domain along the hydro-

phobic linker so that the β-helix and catalytic domain would be in a nearly collinear orientation (Supporting Information Figure S4, middle panel). In this structure, however, a loop−helix−loop motif spanning residues Asp_{522} to Pro_{574} is still protruding from the toxin. Because reorientation of the N-terminal catalytic domain disrupts several hydrogen bonds between the catalytic domain and this loop−helix−loop motif (e.g., residues Asn_{680} and Ser_{139}; Lys_{679} and Thr_{136}; Ala_{576} and Asp_{67}; and Lys_{582} and Ser_{215}), the hinge-like repositioning of the catalytic domain may result in additional conformational changes to the loops connecting the Thr_{580}−Asn_{585} α-helix to the β-helix core structure (Supporting Information Figure S4, right panel). These linked structural changes could thus alleviate the steric barrier to Pet passage through the 60 Å pore of the Sec61 translocon. In regard to this model, translocation of hemoglobin protease across the *E. coli* outer membrane has recently been suggested to involve a hingelike movement of the catalytic domain to a position below the β-helix (*32*).

The absence of secondary structure within the putative Pet hinge/linker region would provide a degree of structural flexibility to the secreted toxin that could conceivably allow it to enact a chaperone-assisted pivot mechanism in the ER lumen. Other SPATEs appear to contain α-helical secondary structure within their linker domains, but none of these autotransporters contact the ER or the ERAD system (Supporting Information Figure S5). The secreted autotransporter toxin of uropathogenic *E. coli* is the one exception to this observation: like Pet, it is predicted to have an unstructured linker between its β-helix domain and catalytic domain. However, Pet and the secreted autotransporter toxin are both internalized by host cells before they disrupt the actin cytoskeleton through proteolysis of α-fodrin and possibly other substrates (*33*). It is therefore likely that Pet and the secreted autotransporter toxin both enter the cytosol by crossing the ER membrane. The absence of secondary structure within the SPATE linker domain could thus be functionally significant for toxin passage from the ER to the cytosol.

After passing through the Sec61 translocon, toxin refolding would likely be required for Pet to act upon its cytosolic fodrin target. The loss of Pet tertiary structure that occurs upon sample heating up to ∼50 °C is reversible and does not eliminate toxin activity against cultured cells. This indicates that the toxin can regain its native conformation after partial unfolding, such as might occur during export to the cytosol. Our protease sensitivity assay further suggests that the interaction between Pet and fodrin may alter and stabilize the conformation of Pet. Similar stabilizing interactions between toxin A chains and specific cytosolic cofactors or targets have been reported (*10*−*12*).

Autotransporters are a diverse family of virulence factors with similar β-helix structural motifs. Here, we examined how host−toxin interactions are influenced by the structure of the Pet autotransporter. Our data indicate that the structure of Pet has evolved to manipulate the ERAD translocation pathway by a process distinct from the mechanism utilized by AB-type, ER-translocating toxins.

ACKNOWLEDGMENT

We thank Dr. Ron Prywes (Columbia University, New York, NY) for the kind gift of plasmid 5xATF6GL3.

SUPPORTING INFORMATION AVAILABLE

The FTIR data on temperature-induced structural changes in Pet, as well as the computer-modeled structures of Pet and SPATE proteins. This material is available free of charge via the Internet at http://pubs.acs.org.

REFERENCES

1. Canizalez-Roman, A., and Navarro-Garcia, F. (2003) Fodrin CaM-binding domain cleavage by Pet from enteroaggregative *Escherichia coli* leads to actin cytoskeletal disruption. *Mol. Microbiol. 48*, 947–958.
2. Henderson, I. R., Hicks, S., Navarro-Garcia, F., Elias, W. P., Philips, A. D., and Nataro, J. P. (1999) Involvement of the enteroaggregative *Escherichia coli* plasmid-encoded toxin in causing human intestinal damage. *Infect. Immun. 67*, 5338–5344.
3. Navarro-Garcia, F., Eslava, C., Villaseca, J. M., Lopez-Revilla, R., Czeczulin, J. R., Srinivas, S., Nataro, J. P., and Cravioto, A. (1998) In vitro effects of a high-molecular-weight heat-labile enterotoxin from enteroaggregative *Escherichia coli*. *Infect. Immun. 66*, 3149–3154.
4. Henderson, I. R., Navarro-Garcia, F., Desvaux, M., Fernandez, R. C., and Ala'Aldeen, D. (2004) Type V protein secretion pathway: the autotransporter story. *Microbiol. Mol. Biol. Rev. 68*, 692–744.
5. Navarro-Garcia, F., Canizalez-Roman, A., Vidal, J. E., and Salazar, M. I. (2007) Intoxication of epithelial cells by plasmid-encoded toxin requires clathrin-mediated endocytosis. *Microbiology 153*, 2828–2838.
6. Navarro-Garcia, F., Canizalez-Roman, A., Burlingame, K. E., Teter, K., and Vidal, J. E. (2007) Pet, a non-AB toxin, is transported and translocated into epithelial cells by a retrograde trafficking pathway. *Infect. Immun. 75*, 2101–2109.
7. Navarro-Garcia, F., Canizalez-Roman, A., Luna, J., Sears, C., and Nataro, J. P. (2001) Plasmid-encoded toxin of enteroaggregative *Escherichia coli* is internalized by epithelial cells. *Infect. Immun. 69*, 1053–1060.
8. Romisch, K. (1999) Surfing the Sec61 channel: bidirectional protein translocation across the ER membrane. *J. Cell Sci. 112* (Part 23), 4185–4191.
9. Sandvig, K., and van Deurs, B. (2002) Membrane traffic exploited by protein toxins. *Annu. Rev. Cell Dev. Biol. 18*, 1–24.
10. Argent, R. H., Parrott, A. M., Day, P. J., Roberts, L. M., Stockley, P. G., Lord, J. M., and Radford, S. E. (2000) Ribosome-mediated folding of partially unfolded ricin A-chain. *J. Biol. Chem. 275*, 9263–9269.
11. Pande, A. H., Moe, D., Jamnadas, M., Tatulian, S. A., and Teter, K. (2006) The pertussis toxin S1 subunit is a thermally unstable protein susceptible to degradation by the 20S proteasome. *Biochemistry 45*, 13734–13740.
12. Pande, A. H., Scaglione, P., Taylor, M., Nemec, K. N., Tuthill, S., Moe, D., Holmes, R. K., Tatulian, S. A., and Teter, K. (2007) Conformational instability of the cholera toxin A1 polypeptide. *J. Mol. Biol. 374*, 1114–1128.
13. Deeks, E. D., Cook, J. P., Day, P. J., Smith, D. C., Roberts, L. M., and Lord, J. M. (2002) The low lysine content of ricin A chain reduces the risk of proteolytic degradation after translocation from the endoplasmic reticulum to the cytosol. *Biochemistry 41*, 3405–3413.
14. Rodighiero, C., Tsai, B., Rapoport, T. A., and Lencer, W. I. (2002) Role of ubiquitination in retro-translocation of cholera toxin and escape of cytosolic degradation. *EMBO Rep. 3*, 1222–1227.
15. Worthington, Z. E., and Carbonetti, N. H. (2007) Evading the proteasome: absence of lysine residues contributes to pertussis toxin activity by evasion of proteasome degradation. *Infect. Immun. 75*, 2946–2953.
16. Donato, H., Jr., Mani, R. S., and Kay, C. M. (1991) Spectral [corrected] studies on the cadmium-ion-binding properties of bovine brain S-100b protein. *Biochem. J. 276* (Part 1), 13–8.
17. Wang, Y., Shen, J., Arenzana, N., Tirasophon, W., Kaufman, R. J., and Prywes, R. (2000) Activation of ATF6 and an ATF6 DNA binding site by the endoplasmic reticulum stress response. *J. Biol. Chem. 275*, 27013–27020.
18. Otto, B. R., Sijbrandi, R., Luirink, J., Oudega, B., Heddle, J. G., Mizutani, K., Park, S. Y., and Tame, J. R. (2005) Crystal structure

of hemoglobin protease, a heme binding autotransporter protein from pathogenic *Escherichia coli*. *J. Biol. Chem. 280*, 17339–17345.
19. Lambert, C., Leonard, N., De Bolle, X., and Depiereux, E. (2002) ESyPred3D: Prediction of proteins 3D structures. *Bioinformatics 18*, 1250–1256.
20. Renn, J. P., and Clark, P. L. (2008) A conserved stable core structure in the passenger domain beta-helix of autotransporter virulence proteins. *Biopolymers 89*, 420–427.
21. Cantor, C. R., and Schimmel, P. R. (1980) Part II: Techniques for the study of biological structure and function, in *Biophysical Chemistry*, W. H. Freeman and Co., New York.
22. Lakowicz, J. R. (1999) *Principles of Fluorescence Spectroscopy*, 2nd ed., Kluwer Academic/Plenum Publishers, New York.
23. Permyakov, S. E., Bakunts, A. G., Denesyuk, A. I., Knyazeva, E. L., Uversky, V. N., and Permyakov, E. A. (2008) Apo-parvalbumin as an intrinsically disordered protein. *Proteins*. doi: 10.1002/prot.21974.
24. Sreerama, N., and Woody, R. W. (2000) Circular dichroism of peptides and proteins, in *Circular Dichroism: Principles and Applications* (Berova, N., Nakanishi, K., and Woody, R. W., Eds.) pp 601−620, John Wiley & Sons, Inc., Hoboken, NJ.
25. Woody, R. W., and Dunker, A. K. (1996) Aromatic and cysteine side-chain circular dichroism in proteins, in *Circular Dichroism and the Conformational Analysis of Biomolecules* (Fasman, G. D., Ed.) pp 109−157, Plenum Press, New York and London.
26. Romisch, K. (2004) A cure for traffic jams: small molecule chaperones in the endoplasmic reticulum. *Traffic 5*, 815–820.
27. Sandvig, K., Madshus, I. H., and Olsnes, S. (1984) Dimethyl sulphoxide protects cells against polypeptide toxins and poliovirus. *Biochem. J. 219*, 935–940.
28. Nagaya, H., Tamura, T., Higa-Nishiyama, A., Ohashi, K., Takeuchi, M., Hashimoto, H., Hatsuzawa, K., Kinjo, M., Okada, T., and Wada, I. (2008) Regulated motion of glycoproteins revealed by direct visualization of a single cargo in the endoplasmic reticulum. *J. Cell Biol. 180*, 129–143.
29. Bernales, S., Papa, F. R., and Walter, P. (2006) Intracellular signaling by the unfolded protein response. *Annu. Rev. Cell Dev. Biol. 22*, 487–508.
30. Navarro-Garcia, F., Sears, C., Eslava, C., Cravioto, A., and Nataro, J. P. (1999) Cytoskeletal effects induced by pet, the serine protease enterotoxin of enteroaggregative *Escherichia coli*. *Infect. Immun. 67*, 2184–2192.
31. Hamman, B. D., Chen, J. C., Johnson, E. E., and Johnson, A. E. (1997) The aqueous pore through the translocon has a diameter of 40−60 A during cotranslational protein translocation at the ER membrane. *Cell 89*, 535–544.
32. Jong, W. S., ten Hagen-Jongman, C. M., den Blaauwen, T., Jan Slotboom, D., Tame, J. R., Wickstrom, D., de Gier, J. W., Otto, B. R., and Luirink, J. (2007) Limited tolerance towards folded elements during secretion of the autotransporter Hbp. *Mol. Microbiol. 63*, 1524–1536.
33. Maroncle, N. M., Sivick, K. E., Brady, R., Stokes, F. E., and Mobley, H. L. (2006) Protease activity, secretion, cell entry, cytotoxicity, and cellular targets of secreted autotransporter toxin of uropathogenic *Escherichia coli*. *Infect. Immun. 74*, 6124–6134.
34. Day, P. J., Pinheiro, T. J., Roberts, L. M., and Lord, J. M. (2002) Binding of ricin A-chain to negatively charged phospholipid vesicles leads to protein structural changes and destabilizes the lipid bilayer. *Biochemistry 41*, 2836–2843.

BI8008714